Axially Nonadiabatic Channel Treatment of Low-Energy Capture in Ion-Rotating Diatom Collisions†

E. I. Dashevskaya,‡ I. Litvin,‡,§ E. E. Nikitin,‡,§ I. Oref,‡ and J. Troe*,§

Department of Chemistry, Technion-Israel Institute of Technology, Haifa, 32000 Israel, and Institut für Physikalische Chemie der Universität Göttingen, Tammannstrasse 6, D-37077 Göttingen, Germany

Received: January 28, 2004; In Final Form: March 24, 2004

The quantum version of an axially nonadiabatic channel (ANC) approximation, introduced in an earlier article for the calculation of complex-formation cross sections and rate constants in ion−diatom collisions [Maergoiz, A. I.; Nikitin, E. E.; Troe, J.; Ushakov, V. G. *J. Chem. Phys*. **2002**, *117*, 4201−4213] is tested against accurate quantum results. Cross sections and rate constants are determined for several representative systems with the participation of a diatom in the state $j = 1$, assuming various long-range potentials between the collision partners, such as anisotropic ion-induced dipole, second-order charge-permanent dipole, and first-order charge−quadrupole interaction. The ANC approximation well reproduces accurate quantum results in the perturbed rotor limit, while the standard quantum adiabatic channel (AC) approximation fails at low energy due to neglect of Coriolis coupling. However, the low-energy extrapolation of classical adiabatic channel results (ACCl) provides a reasonable approximation both to accurate and quantal ANC results down to collision energies when only few partial cross sections determine the total capture cross section. This unexpected feature of the ACCl approximation is due to two effects: (a) an artificial simulation of tunneling transmission and overbarrier reflection at centrifugal barriers by introducing a continuous distribution over total angular momenta and (b) a slight effective lowering of the centrifugal barriers compared to centrifugal barriers within the AC model. Low-temperature quantum rate constants are also presented.

1. Introduction

The calculation of cross sections and rate constants for complex formation in molecular collisions at low energies and temperatures represent an important problem of chemical kinetics. The full quantum treatment of this problem requires the solution of the Schroedinger equation for several degrees of freedom with absorbing boundary conditions for the relative motion. The main complication in accurate quantum calculations is related to the coupling of internal molecular motion to the relative motion. In an attempt to simplify this part of the problem, the so-called adiabatic channel (AC) approximation has been suggested (for a review see ref 1). It has been implemented mainly under the additional condition that the relative motion of partners can be regarded as classical.[2,3] The next step beyond the AC approximation consists of a partial account for nonadiabatic transitions.

For not too low collision energies, the capture cross section is dominated by contributions from large values of the total angular momentum quantum numbers. In this case, the noticeable nonadiabatic effects fall into two main categories: one corresponds to rotational (Coriolis) coupling between AC states converging to a common asymptotic limit, and the other, to radial coupling between AC states whose potential curves display narrow avoided crossings. The regions of asymptotic rotational coupling are located quite far from the regions where the system overcomes centrifugal barriers. The latter condition is crucial for a good performance of the AC approximation in the treatment of complex formation in collisions of rotationally unpolarized partners.[4] Nonadiabatic transitions due to radial coupling that occur in localized regions of avoided crossing have been incorporated into a general AC scheme,[2,3] and their generalizations for globally nonadiabatic situations were studied in the so-called "post-adiabatic" framework.[5] Rotationally induced nonadiabatic transitions in the asymptotic region were also studied in detail in connection with polarization aspects,[6] while the effects of rotationally nonadiabatic coupling in the region of the barriers were taken into account within an axially nonadiabatic channel (ANC) approximation.[7]

For low collision energies, the capture cross section is made up of small numbers of partial contributions. Since the total angular momenta of each partial cross section are not large, the region of the centrifugal barriers may be close to the region of the rotational coupling. In this situation, the transition through the potential barrier is essentially nonadiabatic. It may seem that the adiabatic approximation performs better for decreasing collision energy. This is indeed so for collision partners that do not possess intrinsic angular momenta: in this case the complex-formation cross section can be calculated as a capture cross section in a field of isotropic potentials[8] which permits a rather simple approach of zero collision energies. However, if the intrinsic angular momenta are not zero, the rotational coupling persists down to zero collision energies and may considerably modify the AC capture cross section for low energies. The inapplicability of the AC approximation to low collision energies becomes apparent by the fact that the zero-energy behavior of the AC capture cross contradicts the universal Bethe law, which predicts an inverse velocity dependence of the cross section.[9]

† Part of the "Gert D. Billing Memorial Issue".
‡ Technion-Israel Institute of Technology.
§ Institut für Physikalische Chemie der Universität Göttingen.

10.1021/jp040084o CCC: $27.50
Published on Web 05/04/2004

Indeed, in the AC approximation, the centrifugal potential $C^{J,\tilde{\omega},\mathrm{AC}}$ for an AC state with the quantum numbers $J,\tilde{\omega}$ (J and $\tilde{\omega}$ are the quantum numbers of the total angular momentum and its projection onto the collision axis) is $C^{J,\tilde{\omega},\mathrm{AC}} = \hbar^2\langle\hat{\mathbf{l}}^2\rangle_{J,\tilde{\omega}}/2\mu R^2$ where $\hat{\mathbf{l}}$ is the operator of the relative angular momentum, μ is the reduced mass of the fragments, and R is their center-of-mass separation. Because of the coupling of angular momenta, the minimum of the expectation value of $\hat{\mathbf{l}}^2$ is positive, which signals a deviation from the inverse velocity law. This also indicates that Coriolis coupling plays a decisive part in the low-energy capture event and raises the question whether the ANC approximation can adequately describe the recoupling of angular momenta in the collision event. If the answer is positive, it means a drastic reduction of computational efforts in the calculation of capture cross sections. Indeed, the hierarchy of these efforts, for different levels of approximation, is the following: The AC approximation requires the diagonalization of the block-diagonal interaction matrix with the collision axis as the quantization axis at fixed interparticle distances, and the ANC approximation requires the diagonalization of the interaction matrix together with the Coriolis coupling at fixed interparticle distances, while the full dynamical treatment requires the solution of the scattering equations.

The objective of this paper is to study the performance of the AC and ANC approximations for the calculation of low-energy capture cross sections of a simple system which includes angular momentum recoupling. We thus consider a system consisting of an ion interacting with a diatomic molecule in a rotational state with $j = 1$, assuming various types of long-range anisotropic interaction (anisotropic ion−induced dipole, first-order ion−molecular quadrupole, and second-order ion−molecular dipole interactions). In our treatment, we go beyond alternative adiabatic channel studies of rotationally selected ion−dipole collisions which all have neglected Coriolis coupling effects such as refs 10−17 and, therefore, are not suitable for low-temperature applications.

The plan of the presentation is as follows. In section 2, we review some theoretical background for the calculation of cross sections and rate coefficients. In section 3, we consider adiabatic channel states and couplings for a system $A^+ + BC(j = 1)$. In section 4, we discuss the classical limit of quantum rate coefficients. Section 5 is devoted to the Bethe limit for capture cross sections and rate coefficients. Section 6 presents a bridging between AC and Bethe limits for four representative systems, i.e., $H_2 + Ar^+$, $N_2 + He^+$, $CO + He^+$, and $HCl + H_3^+$. A conclusion finally summarizes the results obtained.

2. Theoretical Background

We consider the collision of a structureless particle A (an atomic ion in a closed electronic state) with a rigid rotor BC in a given rotational state with quantum number j; a rigid rotor is a fair approximation to a real diatomic molecule in a closed electronic state if the vibrational motion is adiabatically separated from other degrees of freedom. We assume a long-range anisotropic interaction $V(R,\gamma)$ where R is the distance between A and the center-of-mass of BC, γ is the angle between the molecular axis and the collision axis **R**.

A complex ABC is assumed to be formed when the partners approach each other to a certain "capture" distance R_c. The dynamics of complex formation is described by a wave function which is the solution of the Schroedinger equation with a potential whose long-range part is $V(R,\gamma)$. The boundary conditions for the wave function are an incoming plane wave and an outgoing spherical wave at large R and complete absorption at the complex surface, i.e., at $R = R_c$. The asymptotics of the wave function furnishes complex-formation (capture) probabilities P_{jl}^J labeled by the quantum numbers of the total angular momentum J, the relative angular momentum l, and intrinsic angular momentum j. The state-specific complex-formation cross section for a rotationally unpolarized molecule is given by the standard formula for inelastic cross sections (see, e.g., ref 18) in which the absolute values of the squared matrix elements of the scattering matrix are replaced by the capture probabilities:

$$\sigma_j(k) = \frac{\pi}{k^2}\sum_{l,J}\frac{2J+1}{2j+1}P_{j,l}^{J,(p)}(k) \tag{1}$$

Here k is the wave vector which is related to the collision energy E and the relative velocity v through $E = \hbar^2k^2/2\mu = \mu v^2/2$ with μ being the reduced mass of the partners.

The wave function in jlJ representation possesses a definite parity p which is conserved; however, for a given set jlJ, it is redundant, and therefore, in eq 1 it appears in parentheses. Instead of the jlJ representation, one can use the $j\tilde{\Omega}J$ representation with $\tilde{\Omega}$ being the quantum number of the projection of **j** onto **R** at $R \to \infty$ (the so-called R-helicity representation). A wave function in $j\tilde{\Omega}J$ representation does not possess a definite parity, but can be made so, if the signed quantities $\tilde{\Omega}$ are replaced by their absolute value $\Omega = |\tilde{\Omega}|$ and the parity. Since the transformation $jlJ \leftrightarrow j\Omega pJ$ is unitarian, eq 1 can be rewritten as

$$\sigma_j(k) = \frac{\pi}{k^2}\sum_{\Omega,p,J}\frac{2J+1}{2j+1}P_{j,\Omega}^{J,p}(k) \tag{2}$$

In our calculations of capture probabilities, we make some assumptions which are appropriate for low-energy collisions and practically interesting cases:

(i) An initial rotational state j is adiabatically isolated from other rotational states.

(ii) The interaction anisotropy is not too weak, such that in the region of the potential well the standard AC approximation holds.

(iii) The interaction in the region of the potential well is strong enough, such that the motion inside the well is quasiclassical (it may not be such in the region of the long-range part of the potential).

Within assumption i, the scattering problem is formulated in terms of $2j + 1$ coupled radial equations; assumption ii means that in the region of strong interaction there exists a good quantum number $\tilde{\omega}$, the projection of **j** onto the collision axis **R**; finally, assumption iii permits a simple formulation of the absorbing boundary condition. The above assumptions allow one to get, besides numerical results, valuable analytical formulas which shed light on general features of capture dynamics in anisotropic situations.

If assumption i is not valid, we have to consider the quantum-scattering problem in full by purely numerical means, or, at elevated collision energies, to resort to classical trajectory calculations. The latter has been used extensively in ref 3. If assumption ii is not valid, the situation is close to the capture in an isotropic potential which was elaborated recently.[7] If assumption iii is not valid, this usually means such a weak attraction that the complex-formation cross section is so small that it is of no practical interest.

An AC version of capture theory assumes that the projection quantum number $\tilde{\omega}$ of **j** onto the collision axis remains a good

TABLE 1: Parameters of Several Ion−Diatom Systems (Data from References 19 and 20)

system	α, au	*Q*, au	μ_D, au	R_L, au	*B*, au	*a*	*b*	E_L, au
$H_2 + Ar^+$	5.437	0.474	0	138	2.7×10^{-4}	−0.052	4.81	1.501×10^{-8}
$N_2 + He^+$	11.74	−1.09	0	274	9.12×10^{-6}	−0.054	−10.20	2.087×10^{-9}
$CO + He^+$	13.36	−1.86	0.048	292	8.75×10^{-6}	1.93	−16.25	1.827×10^{-9}
$HCl + H_3^+$	17.55	2.8	0.436	299	4.83×10^{-5}	22.5	19.1	2.204×10^{-9}

quantum number for arbitrary *R* and considers one-dimensional radial motion across the effective AC potentials $U_{\tilde{\omega}}^{J,AC,eff}(R)$. As explained in ref 4, this assumption, if taken literally, is not valid since the AC functions $|j,\tilde{\omega}\rangle$ undergo a strong nonadiabatic transformation (the so-called locking phenomenon) before, with increase of *R*, they reach the asymptotic region where $\tilde{\omega}$ becomes identical to $\tilde{\Omega}$. However, if the collisions are quasiclassical, two regions, one for the barrier transmission and another for the locking, are well separated, and the AC version of eq 2 can be rewritten as

$$\sigma_j^{AC}(k) = \frac{\pi}{k^2} \sum_{\omega,p,J} \frac{2J+1}{2j+1} P_{j,\omega}^{J,p,AC}(k) \tag{3}$$

where $P_{j,\omega}^{J,p,AC}$ are the transmission probabilities through the centrifugal barriers of the effective radial potential $U_{\omega}^{J,AC,eff}(R)$ (note that $U_{\omega}^{J,AC,eff}(R)$ do not depend on *p*).

An ANC version of capture theory assumes that the radial motion is adiabatic in the field of the ANC effective potentials $U_n^{J,ANC,eff}(R)$. The latter are obtained as eigenvalues (subscript *n* numbers these eigenvalues for fixed *J* and *j*) of the matrix composed of $U_{\tilde{\omega}}^{J,AC,eff}(R)$ and the Coriolis interaction. In ANC approximation, eq 2 assumes the form

$$\sigma_j^{ANC}(k) = \frac{\pi}{k^2} \sum_{n,J} \frac{2J+1}{2j+1} P_{j,n}^{J,ANC}(k) \tag{4}$$

Here the $P_{j,n}^{J,ANC}$ are calculated as transmission probabilities through the centrifugal barriers of $U_n^{J,ANC,eff}(R)$.

In what follows, we assume a generic type of an attractive anisotropic interaction, an anisotropic ion-induced dipole interaction, ion−molecular quadrupole interaction, or ion−molecular dipole interaction of the form

$$V(R,\gamma) = -\frac{q^2\alpha}{2R^4} - \frac{q\mu_D}{R^2}\cos\gamma + \left(-\frac{q^2\Delta\alpha}{3R^4} + \frac{qQ}{R^3}\right)P_2(\cos\gamma) \tag{5}$$

where *q* is the charge of the ion, α is the mean polarizability, $\alpha = (\alpha_{||} + 2\alpha_{\perp})/3$, $\Delta\alpha = \alpha_{||} - \alpha_{\perp}$, μ_D is the permanent dipole moment, and *Q* is the quadrupole moment of the molecule.

In the perturbed rotor approximation, eq 5 yields the following AC potentials (see refs 19 and 20) for second-order ion−dipole interaction, for first-order ion−quadrupole, and anisotropic ion-induced dipole interaction:

$$V_{j,\tilde{\omega}}^{AC}(R) = -\frac{q^2\alpha}{2R^4} + \left(-\frac{q^2\Delta\alpha}{3R^4} + \frac{qQ}{R^3} + \frac{q^2\mu_D^2}{4BR^4}\right) \times \langle j,\tilde{\omega}|P_2(\cos\gamma)|j,\tilde{\omega}\rangle \tag{6}$$

where *B* is the rotational constant of the diatomic molecule (in energy units). The perturbed-rotor approximation for the capture event is valid provided that two dimensionless parameters, $\lambda_{quad} = 3qQ/2BR_{max}^3$ and $\lambda_{dip} = q\mu_D/BR_{max}^2$, which measure the relative strength of the interaction at the maximum of the innermost centrifugal barrier (at $R = R_{max}$), are noticeably smaller than unity.

The information contained in eq 6 is sufficient to calculate cross sections in AC approximation. However, for the ANC approaches and accurate calculations, one has to know the interchannel coupling.

The state-specific capture cross sections lead to energy-dependent state specific rate coefficients $K_j(E)$ and temperature-dependent state-specific rate constants $\bar{K}_j(T)$ which are related to the cross sections $\sigma_j(k)$ in a standard way:

$$K_j(E) = \sqrt{\frac{2E}{\mu}}\sigma_j(E); \quad \bar{K}_j(T) = \langle K_j(k)\rangle_T \tag{7}$$

where $\langle ...\rangle_T$ denotes averaging over the Maxwell distribution in the relative kinetic energies.

3. Adiabatic Channel Potentials, Adiabatic States, and Nonadiabatic Coupling for Perturbed Rotor States with $j = 1$

In what follows, we consider perturbed rotor states that originate from the rotational state $j = 1$ of a diatom. Since *j* is fixed, we suppress super/subscripts *j* in all expressions. We also introduce scaled interparticle distances $\rho = R/R_L$, scaled wave vectors $\kappa = kR_L$, and scaled energies $\epsilon = E/E_L$with $R_L = \sqrt{q^2\alpha\mu}/\hbar$ and $E_L = \hbar^2/\mu R_L^2$. With this convention, the scaled AC potentials $v_{\omega}^{AC}(\rho)$ read as follows:[19,20]

$$v_{\omega}^{AC} = \frac{V_{j,\omega}^{AC}|_{j=1}}{E_L} = -\frac{1}{2\rho^4} + \frac{1}{2}\left(\frac{a}{\rho^4} + \frac{b}{\rho^3}\right)(2 - 3\omega^2) \tag{8}$$

Here the first term on the rhs represents the scaled ion-induced dipole isotropic interaction. The rest, originating from the anisotropic part, contains two interaction parameters: parameter *a* encompasses the scaled ion-induced dipole anisotropic interaction and the second-order ion−molecular dipole interaction whereas the parameter b results from the first-order ion−molecular quadrupole interaction. The explicit expressions of *a*,*b* in terms of the parameters entering in eq 8 are

$$a = 2\Delta\alpha/15\alpha + \mu_D^2/10\alpha B, \quad b = 2\mu qQ/5R_L\hbar^2 \tag{9}$$

Table 1 presents values of the dimensionless parameters *a* and *b* for several ion−diatom systems together with the relevant molecular parameters.

The AC potentials lead to the effective AC potentials that include the centrifugal energy:[21]

$$v_{\omega}^{J,AC,eff}(\rho) = \frac{J(J+1) - 2\omega^2 + 2}{2\rho^2} + v_{\omega}^{AC}(\rho) \tag{10}$$

Note that all effective AC potentials are repulsive at large ρ. The weakest centrifugal repulsion occurs for $v_0^{0,AC,eff}(\rho) \approx v_1^{1,AC,eff}(\rho) \approx 1/\rho^2$. The nonadiabatic coupling between the three AC states under discussion, $|0\rangle$, $|1\rangle$, $|-1\rangle$ for $\omega = 0, +1, -1$, is of the Coriolis type. The description of this coupling is simplified when one uses a basis with definite parity. Let the latter states be $|0\rangle$, $|1\rangle$, $|\bar{1}\rangle$ where the states $|0\rangle$, $|1\rangle$ belong to the same parity while the state $|\bar{1}\rangle$ corresponds to opposite parity.

In the parity-adopted basis, the AC potentials are the same, while the coupling occurs between the states $|0\rangle$ and $|1\rangle$ only, and the coupling off-diagonal interaction is[21]

$$v_{10}^{J,\mathrm{AC,Cor}}(\rho) = \frac{\sqrt{J(J+1)}}{\rho^2} \tag{11}$$

The general wave function Ψ^J, that describes the perturbed rotation of the diatom and the relative radial motion of the ion−diatom, is of the form

$$\Psi^J = |0\rangle\psi_0^J + |1\rangle\psi_1^J + |\bar{1}\rangle\psi_{\bar{1}}^J \tag{12}$$

where the components ψ_0^J, ψ_1^J, $\psi_{\bar{1}}^J$ satisfy the following equations

$$\begin{aligned}
&-\frac{\mathrm{d}^2\psi_0^J}{\mathrm{d}\rho^2} + 2v_0^{J,\mathrm{AC,eff}}\,\psi_0^J - \kappa^2\psi_0^J = 2v_{01}^{J,\mathrm{AC,Cor}}\,\psi_1^J \\
&-\frac{\mathrm{d}^2\psi_1^J}{\mathrm{d}\rho^2} + 2v_1^{J,\mathrm{AC,eff}}\,\psi_1^J - \kappa^2\psi_1^J = 2v_{10}^{J,\mathrm{AC,Cor}}\,\psi_0^J \\
&-\frac{\mathrm{d}^2\psi_{\bar{1}}^J}{\mathrm{d}\rho^2} + 2v_{\bar{1}}^{J,\mathrm{AC,eff}}\,\psi_{\bar{1}}^J - \kappa^2\psi_{\bar{1}}^J = 0
\end{aligned} \tag{13}$$

for $J > 0$ and

$$-\frac{\mathrm{d}^2\psi_0{}^0}{\mathrm{d}\rho^2} + 2v_0^{0,\mathrm{AC,eff}}\psi_0{}^0 - \kappa^2\psi_0^0 = 0 \tag{14}$$

for $J = 0$.

By a rotation of the AC basis one can diagonalize the matrix composed of the effective AC potentials and the Coriolis coupling. The new states, called axially nonadiabatic channel (ANC) states $|a\rangle$, $|b\rangle$, $|c\rangle$, are related to the AC states by

$$\begin{aligned}
&|a\rangle = \cos\theta\cdot|0\rangle + \sin\theta\cdot|1\rangle \\
&|b\rangle = -\sin\theta\cdot|0\rangle + \cos\theta\cdot|1\rangle \\
&|c\rangle = |\bar{1}\rangle \\
&\theta \equiv \theta^J(\rho) = \frac{1}{2}\arctan\frac{2v_{01}^{J,\mathrm{AC,Cor}}}{\Delta v_{01}^{J,\mathrm{AC,eff}}} \\
&\Delta v_{01}^{J,\mathrm{AC,eff}} = v_0^{J,\mathrm{AC,eff}} - v_1^{J,\mathrm{AC,eff}} = \frac{1}{\rho^2} + \frac{3}{2}\left(\frac{a}{\rho^4} + \frac{b}{\rho^3}\right)
\end{aligned} \tag{15}$$

This change of the basis transforms the effective AC potentials into the effective ANC potentials

$$\begin{aligned}
v_{a,b}^{J,\mathrm{ANC,eff}} = {}& (1/2)(v_0^{J,\mathrm{AC,eff}} + v_1^{J,\mathrm{AC,eff}}) \mp \\
& (1/2)\sqrt{(\Delta v_{01}^{J,\mathrm{AC,eff}})^2 + 4(v_{01}^{J,\mathrm{AC,Cor}})^2} \\
v_c^{J,\mathrm{ANC,eff}} = {}& v_1^{J,\mathrm{AC,eff}}
\end{aligned} \tag{16}$$

for $J > 0$ and

$$v^{0,\mathrm{ANC,eff}} = v_0^{0,\mathrm{AC,eff}} \tag{17}$$

for $J = 0$. Note that all effective ANC potentials are repulsive at large ρ save $v_a^{1,\mathrm{ANC,eff}}(\rho)$.

The change in the basis functions in eq 15 changes the coupling between the new states. The wave function Ψ^J now is written as

$$\Psi^J = |a\rangle\psi_a^J + |b\rangle\psi_b^J + |c\rangle\psi_c^J \tag{18}$$

where the components ψ_a^J, ψ_b^J, ψ_c^J satisfy the following equations:

$$\begin{aligned}
&-\frac{\mathrm{d}^2\psi_a^J}{\mathrm{d}\rho^2} + 2v_a^{J,\mathrm{ANC,eff}}\,\psi_a^J - \kappa^2\psi_a^J + g^2\psi_a^J = 2\left(g\frac{\mathrm{d}}{\mathrm{d}\rho} + \frac{\mathrm{d}g}{2\mathrm{d}\rho}\right)\psi_b^J \\
&-\frac{\mathrm{d}^2\psi_b^J}{\mathrm{d}\rho^2} + 2v_b^{J,\mathrm{ANC,eff}}\,\psi_b^J - \kappa^2\psi_b^J + g^2\psi_b^J = -2\left(g\frac{\mathrm{d}}{\mathrm{d}\rho} + \frac{\mathrm{d}g}{2\mathrm{d}\rho}\right)\psi_a^J \\
&-\frac{\mathrm{d}^2\psi_c^J}{\mathrm{d}\rho^2} + 2v_c^{J,\mathrm{ANC,eff}}\,\psi_c^J - \kappa^2\psi_c^J = 0
\end{aligned} \tag{19}$$

Here, the coupling between the ANC states $|a\rangle$ and $|b\rangle$ is described by a single function $g^J(\rho)$ which is determined by the rotation angle $\theta^J(\rho)$ in eq 15 (see ref 18):

$$g^J(\rho) = -\frac{d\theta^J(\rho)}{\mathrm{d}\rho} \tag{20}$$

Equations 13 and 19, when solved accurately, yield the same nonadiabatic wave function. The difference between these equations is that eq 13 describes the rotational coupling between AC states, while eq 19 describes the radial coupling between ANC states. On the other hand, an approximate solution to eqs 13 and 19 will yield different results.

Within the AC approximation, the rotational coupling in eq 13 is neglected, so that the asymptotic quantum numbers 0, 1, $\bar{1}$ become exact quantum numbers. Then the approximate function $\Psi^{J,\mathrm{AC}}$ is represented as follows:

$$\Psi^{J,\mathrm{AC}} = |0\rangle\psi_0^{J,\mathrm{AC}} + |1\rangle\psi_1^{J,\mathrm{AC}} + |\bar{1}\rangle\psi_{\bar{1}}^{J,\mathrm{AC}} \tag{21}$$

Here the components satisfy the equations

$$\begin{aligned}
&-\frac{\mathrm{d}^2\psi_0^{J,\mathrm{AC}}}{\mathrm{d}\rho^2} + 2v_0^{J,\mathrm{AC,eff}}\,\psi_0^{J,\mathrm{AC}} - \kappa^2\psi_0^{J,\mathrm{AC}} = 0 \\
&-\frac{\mathrm{d}^2\psi_1^{J,\mathrm{AC}}}{\mathrm{d}\rho^2} + 2v_1^{J,\mathrm{AC,eff}}\,\psi_1^{J,\mathrm{AC}} - \kappa^2\psi_1^{J,\mathrm{AC}} = 0 \\
&-\frac{\mathrm{d}^2\psi_{\bar{1}}^{J,\mathrm{AC}}}{\mathrm{d}\rho^2} + 2v_1^{J,\mathrm{AC,eff}}\,\psi_{\bar{1}}^{J,\mathrm{AC}} - \kappa^2\psi_{\bar{1}}^{J,\mathrm{AC}} = 0
\end{aligned} \tag{22}$$

Equation 22 differs from eq 13 in that the coupling is omitted; i.e., the rhs in the latter is set to zero.

Within the ANC approach, the approximate function $\Psi^{J,\mathrm{ANC}}$ is represented as

$$\Psi^{J,\mathrm{ANC}} = |a\rangle\psi_a^{J,\mathrm{ANC}} + |b\rangle\psi_b^{J,\mathrm{ANC}} + |c\rangle\psi_c^{J,\mathrm{ANC}} \tag{23}$$

where the components satisfy the equations

$$-\frac{d^2\psi_a^{J,ANC}}{d\rho^2}+2v_a^{J,ANC,eff}\psi_a^{J,ANC}-\kappa^2\psi_a^{J,ANC}=0$$
$$-\frac{d^2\psi_b^{J,ANC}}{d\rho^2}+2v_b^{J,ANC,eff}\psi_b^{J,ANC}-\kappa^2\psi_b^{J,ANC}=0 \quad (24)$$
$$-\frac{d^2\psi_c^{J,ANC}}{d\rho^2}+2v_c^{J,ANC,eff}\psi_c^{J,ANC}-\kappa^2\psi_c^{J,ANC}=0$$

Equation 24 differs from eq 19 in that both the coupling (the rhs in the latter) and the diagonal nonadiabatic correction are set to zero.

Equations 13 and 19 describe the quantal coupled propagation of the waves to the absorbing boundary. Equations 22 and 24 describe the uncoupled propagation of the waves, accompanied by the simplest quantal effects, i.e., tunneling through the potential barriers and overbarrier reflection. The equations should be solved with the absorbing boundary conditions on the surface of the complex. Under assumptions ii and iii, these conditions correspond to incoming quasiclassical waves in the potential well, with the presence of a single asymptotic incoming wave in the state with $\omega,p=\Omega,p$. In this way, we get three sets of three probabilities P_0^J, P_1^J, $P_{\bar{1}}^J$, and $P_0^{J,AC}$, $P_1^{J,AC}$, $P_{\bar{1}}^{J,AC}$ and $P_a^{J,ANC}$,$P_b^{J,ANC}$,$P_c^{J,ANC}$ for the accurate, the AC, and the ANC approaches. In turn, these probabilities determine the capture cross sections σ,σ^{AC} and σ^{ANC}.

In what follows, instead of the capture cross sections, we use the energy-dependent rate coefficients defined by eq 7. The scaled version of $K(E)$, $\chi(\kappa)$, is defined as

$$K(k)=\left(2\pi\frac{\hbar}{\mu}R_L\right)\chi(\kappa) \quad (25)$$

where $\chi(\kappa)$ assumes the form

$$\chi(\kappa)=\sum_{J=0}^{\infty}\chi^J(\kappa);\ \chi^J(\kappa)=\frac{(2J+1)}{6\kappa}(P_0^J+P_1^J+P_{\bar{1}}^J) \quad (26)$$

Similar expressions hold for $\chi^{AC}(\kappa)$ or $\chi^{ANC}(\kappa)$ if the set P_0^J,P_1^J, $P_{\bar{1}}^J$ is replaced by its AC or ANC counterparts.

The following properties of the probabilities are worth mentioning:

(a) Since the state $|\bar{1}\rangle$ is not coupled, we have

$$P_{\bar{1}}^J=P_{\bar{1}}^{J,AC}=P_c^{J,ANC} \quad (27)$$

(b) The states $|0\rangle$ and $|1\rangle$ are coupled, and this coupling persists even for large J and κ, i.e., in the classical limit. Therefore, there is no simple relation between the pairs (P_0^J, P_1^J), ($P_0^{J,AC}$, $P_1^{J,AC}$), and ($P_a^{J,ANC}$, $P_b^{J,ANC}$). However, in the classical limit, when the locking of the diatom angular momentum to the collision axis occurs at distances much larger than the location of centrifugal maxima, the following relation holds:

$$P_0^J+P_1^J=P_0^{J,AC}+P_1^{J,AC}=P_a^{J,ANC}+P_b^{J,ANC} \quad (28)$$

Finally we mention that the normalization of $\chi(\kappa)$ is chosen such that, in the case of pure isotropic interaction, i.e., $a=b=0$, the high-energy limit of $\chi(\kappa)$ is unity, and that of $K(k)$ is the Langevin capture rate coefficient $K_L=2\pi\hbar R_L/\mu$.

4. Classical Limit of the Accurate, AC and ANC Rate Coefficients

The classical limit of $\chi(\kappa)$, $\chi^{AC}(\kappa)$, and $\chi^{ACCl}(\kappa)$ is obtained from eq 26 when the summation over J is replaced by integration, the quantum capture probabilities are replaced by the classical capture probabilities $P_\omega(J)$. The latter are given by the step functions

$$P_\omega(\kappa,J)=\theta(\Lambda_\omega(\kappa)-J) \quad (29)$$

where $\Lambda_\omega(\kappa)$ is the maximum angular momentum for which classical capture in the field of the potential $v_\omega(\rho)$ is possible for the collision energy $\kappa^2/2$. The quantity Λ_ω is determined from the classical capture condition:

$$\max\left\{\frac{\Lambda^2}{2\rho^2}+v_\omega^{AC}(\rho)\right\}\Big|_{\Lambda=\Lambda_\omega(\kappa)}=\kappa^2/2 \quad (30)$$

If eq 30 does not yield a solution with positive $\Lambda_\omega{}^2$, this means that capture does not occur. Finally, the properties expressed by eqs 27 and 28 allow one to write the following formulas:

$$\chi(\kappa)|_{\kappa\gg1}=\chi^{AC}(\kappa)|_{\kappa\gg1}=\chi^{ANC}(\kappa)|_{\kappa\gg1}=\chi^{ACCl}(\kappa)$$
$$\chi^{ACCl}(\kappa)=\frac{1}{6\kappa}[(\Lambda_0(\kappa))^2+2(\Lambda_1(\kappa))^2] \quad (31)$$

5. Bethe Limit for Capture Cross Sections and Capture Rate Coefficients

In the Bethe limit, $\kappa\to0$, according to Wigner's arguments,[9,22] the threshold behavior of the transmission probabilities for a given channel is determined by the asymptotics of the centrifugal repulsion in this channel. In general, for low κ, the transmission probabilities are proportional to $\kappa^{1+\delta}$ with $\delta\geq0$. In the limit $\kappa\to0$, only those terms in eq 26 survive for which $\delta=0$.

Within the accurate quantum treatment, this can happen only for the coupled states ψ_0^J and ψ_1^J so that the nonzero contributions to the rate coefficient can only come from P_0^1 and P_1^1. The probabilities P_0^1 and P_1^1 are expected to be linear in κ, and depend on the two interaction parameters a and b. Thus, the low-κ limit of capture probabilities are:

$$P_0^1=C_0^1(a,b)\kappa;\quad P_1^1=C_1^1(a,b)\kappa;\quad P_{\bar{1}}^1=0 \quad (32)$$

where $P_{\bar{1}}^1=0$ means that $P_{\bar{1}}^1$ tends to zero faster than κ. Therefore, the Bethe limit of eq 26 reads as follows:

$$\lim_{\kappa\to0}\chi(\kappa;a,b)=\chi^B(a,b)=\chi^1(\kappa,a,b)|_{\kappa=0}=\frac{1}{2}(C_0^1(a,b)+C_1^1(a,b)) \quad (33)$$

By the same reason, we arrive at the following expression for the Bethe limit of ANC capture probabilities:

$$P_a^{1,ANC}=C_a^1(a,b)\kappa;\ P_b^{1,ANC}=0;\ P_c^{1,ANC}=0 \quad (34)$$

Thus

$$\lim_{\kappa\to0}\chi^{ANC}(\kappa;a,b)=\chi^{B,ANC}(a,b)=\chi^{1,ANC}(\kappa;a,b)|_{\kappa=0}=\frac{1}{2}C_a^1(a,b) \quad (35)$$

Finally, for the AC approximation, we get

$$P_0^{1,AC}=0;\ P_1^{1,AC}=0;\ P_{\bar{1}}^{1,AC}=0 \quad (36)$$

and

$$\lim_{\kappa\to 0}\chi^{\mathrm{AC}}(\kappa;a,b)=\chi^{\mathrm{B,AC}}(a,b)=0 \tag{37}$$

Numerically, the coefficients C_0^1, C_1^1, and $C_1^{1,\mathrm{ANC}}$ can be found by integration of Schroedinger equations for the particular case $J = 1$ in the limit of small κ and subsequent linear extrapolation to $\kappa = 0$. This procedure is simply a special case of what we report in section 6. However, in the present section we discuss an approximate analytical estimation to $C_a^{1,\mathrm{ANC}}(a,b)$, i.e., $C_{a,\mathrm{as}}^{1,\mathrm{ANC}}(a,b)$, based on the asymptotic representation of $v_a^{1,\mathrm{ANC,eff}}(\rho)$.

For an uncoupled wave equation, such as for the ANC potential $v_a^{1,\mathrm{ANC,eff}}(\rho)$, the coefficient $C_a^{1,\mathrm{ANC}}(a,b)$ can be found from solution of this equation for zero energy.[9] Unfortunately, the potential $v_a^{1,\mathrm{ANC,eff}}(\rho)$ is too complicated and does not permit to get a solution in terms of known higher transcendental functions. We, therefore, adopt an approximation to $v_a^{1,\mathrm{ANC,eff}}(\rho)$ which consists of expanding eq 16 up to second order in the anisotropic part of the interaction. The result reads as follows:

$$v_a^{1,\mathrm{ANC,eff}}(\rho)|_{\rho\to\infty}\to v_{a,\mathrm{as}}^{1,\mathrm{ANC,eff}}(\rho)=-\frac{1}{2\rho^4}-\frac{1}{6}\left(\frac{a}{\rho^3}+\frac{b}{\rho^2}\right)^2 \tag{38}$$

The potential in eq 38 contains three different terms, being proportional to ρ^{-4}, ρ^{-5}, and ρ^{-6}. If a single term is present only, the zero-energy wave equation can be solved in terms of Bessel functions.[23] If there are two terms, the zero-energy wave equation can be solved in terms of confluent hypergeometric functions.[24] Presumably, an equation with three terms can be solved in terms of hypergeometric functions. However, instead of trying to get this kind of the solution, we consider a simplified approach which is sufficient for the discussion in the next section.

To this end, we first consider the case when $a = 0$. The potential from eq 38 becomes

$$v_{a,\mathrm{as}}^{1,\mathrm{ANC,eff}}(\rho)=-\frac{1}{2\rho^4}-\frac{b^2}{6\rho^4}=-\frac{1+b^2/3}{2\rho^4} \tag{39}$$

which is a renormalized ion-induced dipole interaction. This simple result is due to the fact that, in the ANC lowest capture channel, the ion−quadrupole interaction (proportional to $1/\rho^3$) is transformed into an ion-induced dipole interaction, being proportional to $1/\rho^4$. The physics of this transformation is explained in our recent article.[25] Referring to our previous results,[8,20] we find

$$C_{a,\mathrm{as}}^1(0,b)=4\sqrt{1+b^2/3} \tag{40}$$

We see that when b is large enough, $b \gg 1$, the expression for $C_{a,\mathrm{as}}^1(0,b)$ becomes $C_{a,\mathrm{as}}^1(0,b)\approx 4b/\sqrt{3}$. This is a manifestation of the prevailing effect of the long-range ion−quadrupole interaction over the shorter range ion-induced dipole interaction in the limit of zero energy. Physically, this means that the approximation $C_{a,\mathrm{as}}^1(0,b)\approx 4b/\sqrt{3}$ for $C_{a,\mathrm{as}}^1(0,b)$ can be generalized for $C_{a,\mathrm{as}}^1(a,b)$ provided $b \gg 1,a$.

We therefore adopt the following approximation for $C_{a,\mathrm{as}}^1(a,b)$:

$$C_{a,\mathrm{as}}^1(a,b)=4\sqrt{1+b^2/3},\quad \text{if } a=0 \tag{41a}$$

$$C_{a,\mathrm{as}}^1(a,b)=4b/\sqrt{3},\quad \text{if } b\gg 1,a \tag{41b}$$

Equation 41a applies to the capture processes $H_2 + Ar^+$ and $N_2 + He^+$, and eq 41b to $CO + He^+$ (vide infra).

6. Bridging between the Bethe and Classical AC Limits

For the calculation of accurate rate coefficients, we have determined transmission probabilities $P_\omega^J(\kappa)$ by explicitly solving coupled wave equations including the Coriolis interaction for several values of the parameters a and b. In parallel, we calculated ANC and AC transmission probabilities by integrating uncoupled wave equations with ANC and AC effective potentials. The calculations were accomplished for a range of the wave vectors within which we get converged results for probabilities up to $J = 6$. For higher J values, the accurate quantum results for the rate coefficients are already close to the classical AC limit. In what follows, we present the results for four systems listed in Table 1.

To show more clearly the partial contributions to the total rate coefficients with increasing wave vector (or collision energy), following our recent article,[8] we present the rate coefficients χ vs the continuous "threshold" angular momentum $\lambda = \lambda_\omega(\kappa)$. The reason for changing the variable from κ to λ is that the plots $\chi = \chi(\lambda)$ better illustrate the threshold behavior of partial rate coefficients than the plots $\chi = \chi(\kappa)$. The function $\lambda_\omega(\kappa)$ is formally defined for an attractive AC potential $v_\omega^{\mathrm{AC}}(\rho)$ by the following equation:

$$\max\left\{\frac{\lambda(\lambda+1)}{2\rho^2}+v_\omega^{\mathrm{AC}}(\rho)\right\}\Bigg|_{\lambda=\lambda_\omega(\kappa)}=\kappa^2/2 \tag{42}$$

The meaning of the function $\lambda_\omega(\kappa)$ becomes clear when one compares eqs 42 and 30 and identifies $\lambda_\omega(\kappa)[\lambda_\omega(\kappa)+1]$ with $\Lambda_\omega^2(\kappa)$. For an isotropic interaction, which was the case in ref 8, the centrifugal energy is proportional to $l(l+1)$; then the continuous function $\lambda_\omega(\kappa)$ smoothly interpolates between discrete values of l, such that the effective potential $l(l+1)/2\rho^2 + v_\omega^{\mathrm{AC}}(\rho)$ becomes classically open for capture at the wave vector κ that satisfies the relation $\lambda_\omega(\kappa) = l$. For an anisotropic interaction, the centrifugal barrier, within the AC basis, is of more complicated form, see eq 10. In this case, the function $\lambda_\omega(\kappa)$ represents the classical counterpart of the effective angular momentum quantum number that enters into the expression for the effective AC potential $v_\omega^{J,\mathrm{AC,eff}}(\rho)$ written in the form in eq 42. This potential becomes classically open at the wave vector $\kappa = \kappa_{\mathrm{th}}$ that satisfies the relation

$$\lambda_\omega(\kappa_{\mathrm{th}})[\lambda_\omega(\kappa_{\mathrm{th}})+1]=J(J+1)-2\omega^2+2 \tag{43}$$

Plots of four functions $\lambda_1^{H_2+Ar^+}$, $\lambda_0^{N_3+He^+}$, $\lambda_0^{CO+He^+}$, $\lambda_1^{HCl+H_3^+}$ vs κ are shown in Figure 1 for $\lambda_\omega \le 6$. These plots can be used to translate the κ dependence of the rate coefficients into their λ dependence (or vice verse) and also for determination of classical threshold values of wave vectors for different AC channels, provided the respective "threshold" values of λ_ω, are calculated first from eq 43. Note that for an isotropic interaction, the "threshold" values of λ are integer numbers, whereas for an anisotropic interaction they may not be integer. Figure 1 is also useful for estimation of number of AC open channels as a function of the wave vector (see the caption to Figure 1).

For the maximum values of λ_ω treated in our calculations ($\lambda_\omega = 6$), we have determined perturbation parameters λ_{dip} and λ_{quad} (see text after eq 6) and found them to be noticeably smaller than 0.1. We, therefore, conclude that the perturbed-rotor approximation is well applicable. Note that the collision energies for $\lambda_\omega = 6$ are $E_{\lambda_1=6}^{H_2+Ar^+} = 0.4$ K, $E_{\lambda_0=6}^{N_2+He^+} = 0.008$ K, $E_{\lambda_0=6}^{CO+He^+}$

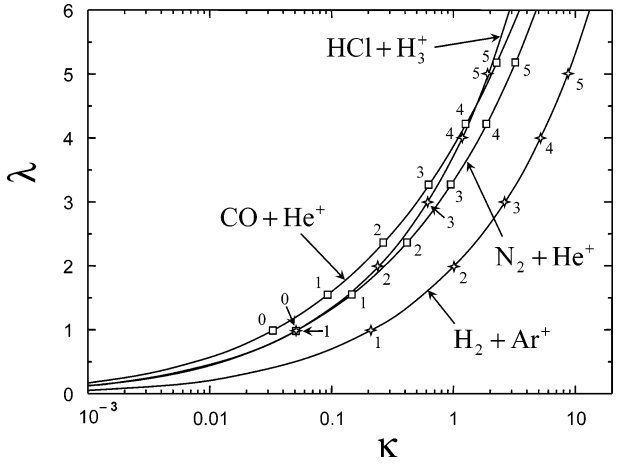

Figure 1. Plots of the functions $\lambda_1^{H_2+Ar^+}$, $\lambda_0^{N_2+He^+}$, $\lambda_0^{CO+He^+}$, $\lambda_1^{HCl+H_3^+}$ vs wave vector κ. Each symbol on a particular curves, marked with the quantum number J, locates the classical AC threshold values $\kappa = \kappa_{th}(J)$ and $\lambda = \lambda_{th}(J)$ that correspond to this J for respective collision. For any given value of κ, the number of AC channels, classically open for capture for a particular collision, is equal to the number of symbols on the appropriate curve in the region bounded by κ from above. For large enough J, $\lambda_{th}(J)$ for all collision pairs cluster around J (AC classical limit).

$= 0.004$ K, $E_{\lambda_1=6}^{HCl+He^+} = 0.003$ K. The much higher value of $E_{\lambda_1=6}$ for $H_2 + Ar^+$ capture compared to that of the other systems is the cumulative effect of smaller reduced mass of the colliding partners and small quadrupole moment of the diatom.

We now consider the above systems in more detail.

Case 1: $H_2 + Ar^+$ *capture, even case, low anisotropic* $1/R^3$ *interaction, very small anisotropic* $1/R^4$ *interaction, and collision energy noticeably below the maximum of* v_0^{AC}.

For this system, the AC potential $v_0^{AC}(\rho)$ is repulsive while $v_{1,\bar{1}}^{AC}(\rho)$ are attractive; therefore, the summation over J in eq 3 begins with $J = 1$. The potentials $v_1^{AC}(\rho)$ and $v_{\bar{1}}^{AC}(\rho)$ are identical; they generate two identical effective potentials, $v_{1,\bar{1}}^{J,AC,eff}(\rho)$. All the effective potentials are repulsive at large ρ, and therefore, the AC rate coefficient vanishes in the limit of small κ or small $\lambda_1(\kappa) = \lambda_{\bar{1}}(\kappa)$.

Within the ANC description, the two effective potentials, $v_0^{J,AC,eff}(\rho)$ and $v_1^{J,AC,eff}(\rho)$ generate two different effective potentials, $v_a^{J,ANC,eff}(\rho)$ and $v_b^{J,ANC,eff}(\rho)$. The third effective ANC potential, $v_c^{J,ANC,eff}(\rho)$, coincides with $v_{\bar{1}}^{J,AC,eff}(\rho)$. The effective potentials $v_a^{J,ANC,eff}(\rho)$ and $v_c^{J,ANC,eff}(\rho)$ are attractive, and $v_b^{J,ANC,eff}(\rho)$ is repulsive. All the ANC effective potentials, save $v_a^{1,ANC,eff}(\rho)$, are repulsive at large ρ; the latter is attractive. Therefore, the contributions to the ANC rate coefficient, $\chi_x^{J,ANC}$ ($x = a, b, c$), vanish in the limit of small κ, save $\chi_a^{J,ANC}$.

Figure 2 shows the comparison of the accurate, χ, and approximate, χ^{AC} and χ^{ANC}, rate coefficients vs $\lambda_1(\kappa)$. Also shown, on the $\lambda_1(\kappa)$ axes, are the classical capture thresholds for the effective AC (lower axis) and ANC (upper axis); the thresholds are marked as $J_{\pm1}$ for the AC potentials, and as J_a, J_c for ANC potentials. We see that χ^{ANC}, for $\lambda_1(\kappa) > 1$, reasonably well approximates the accurate rate coefficient χ. Also, for smaller $\lambda_1(\kappa)$ (e.g., $0.5 < \lambda_1(\kappa) < 1$), where the overwhelming contribution to the capture rate comes from the state $j, l, J = 1, 0, 1$, the ANC approximation is reasonable. The small difference between the accurate and ANC rate coefficients can be ascribed to the neglected radial nonadiabatic coupling between ANC states. Note also that the ANC rate coefficient extrapolates nicely to the theoretical prediction of the Bethe limit which is based on the asymptotic form of

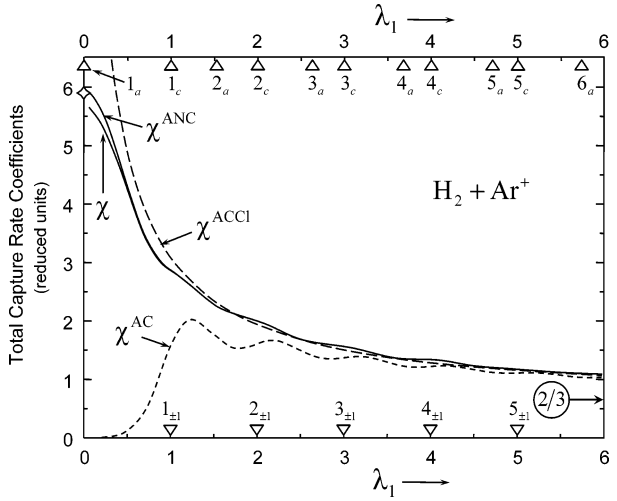

Figure 2. Reduced rate coefficients for $H_2 + Ar^+$ capture. Shown are accurate, ANC, AC, and ACCl rate coefficients, (χ, χ^{ANC}, χ^{AC}, and χ^{ACCl} respectively) vs λ_1. The diamond on the ordinate axis corresponds to the approximate analytical Bethe limit of the rate coefficient. The symbols $J_{\pm1}$, $J = 1, 2, ...$, on the lower λ_1 axis indicate the classical opening of the capture channels for $v_{\pm1}^{J,AC,eff}$ potentials, while the symbols J_a,J_c on the upper λ_1^{AC} axis indicate the classical opening of the capture channels for the $v_a^{J,ANC,eff}$,$v_c^{J,ANC,eff}$ potentials. The ratio $^2/_3$ indicated at the right ordinate axis shows the ion-induced dipole asymptote of χ^{ACCl}.

$\chi_a^{J,ANC}$ (see section 5): $\chi_{as}^{B,ANC} = 2\sqrt{1+b^2/3}$. On the other hand, χ^{AC} breaks down completely for $\lambda_1(\kappa) < 1$ and deviates noticeably from the accurate rate already at $\lambda_1(\kappa) = 3$. At large λ, the accurate and approximate rate coefficients all converge to the classical limit, χ^{ACCl}. For high values of λ_1, the latter is determined mainly by the isotropic ion-induced dipole interaction (very small value of a), and, therefore, converges to $^2/_3$. We see that the rate coefficients at $\lambda_1 = 6$ are about twice as large as their asymptotes which is the manifestation of the ion−quadrupole interaction.

Case 2: $N_2 + He^+$ *capture, an odd case, high anisotropic* $1/R^3$ *interaction, very small anisotropic* $1/R^4$ *interaction, and collision energy noticeably below the maximum of* v_1^{AC}.

Here the AC potentials $v_{1,\bar{1}}^{AC}(\rho)$ are repulsive while $v_0^{AC}(\rho)$ is attractive; therefore, the summation over J in eq 3 begins with $J = 0$. All the effective potentials are repulsive at large ρ, and therefore, the AC rate coefficient vanishes in the limit of small κ.

Within the ANC description, two effective potentials, $v_0^{J,AC,eff}(\rho)$ and $v_1^{J,AC,eff}(\rho)$, generate two different effective potentials, $v_a^{J,ANC,eff}(\rho)$ and $v_b^{J,ANC,eff}(\rho)$. The third effective ANC potential, $v_c^{J,ANC,eff}(\rho)$, coincides with $v_{\bar{1}}^{J,AC,eff}(\rho)$ and is repulsive. All the ANC effective potentials, save $v_a^{1,ANC,eff}(\rho)$, are repulsive at large ρ; the latter is attractive. Therefore, the contributions to the ANC rate coefficient, $\chi_x^{J,ANC}$ ($x = a, b, c$), vanish in the limit of small κ, save $\chi_a^{J,ANC}$.

Figure 3 shows the comparison of the accurate, χ, and approximate, χ^{AC} and χ^{ANC}, rate coefficients vs $\lambda_0(\kappa)$. Also shown, on the $\lambda_0(\kappa)$ axis, are the classical capture thresholds for the effective AC (lower axis) and ANC (upper axis) potentials; the thresholds are marked as J_0 for the AC potentials, and as J_a for ANC potentials. We see that χ^{ANC} approximates reasonably well the accurate rate coefficient χ if $\lambda_0(\kappa)$ is large enough (e.g., for $\lambda_0(\kappa) > 2$). Note also that ANC rate coefficient extrapolates reasonably well to the theoretical prediction based on the asymptotic form of $\chi_a^{J,ANC}$. The AC approximation again

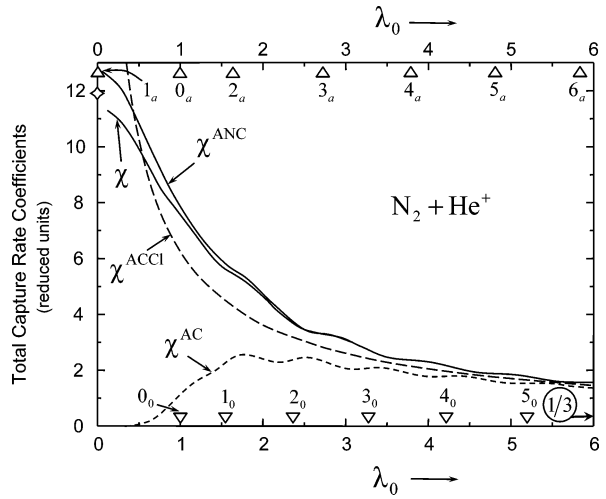

Figure 3. Reduced rate coefficients for $N_2 + Ar^+$ capture. Shown are accurate, ANC, AC, and ACCl rate coefficients, (χ, χ^{ANC}, χ^{AC}, and χ^{ACCl} respectively) vs λ_0. The diamond on the ordinate axis corresponds to the approximate analytical Bethe limit of the rate coefficient. The symbols J_0, $J = 1, 2, ...$, on the lower λ_0 axis indicate the classical opening of the capture channels for the $v_0^{J,AC,eff}$ potential, while the symbols J_a on the upper λ_0 axis indicate the classical opening of the capture channels for the $v_a^{J,ANC,eff}$ potential. The ratio $^1/_3$ indicated at the right ordinate axis shows the ion-induced dipole asymptote of χ^{ACCl}.

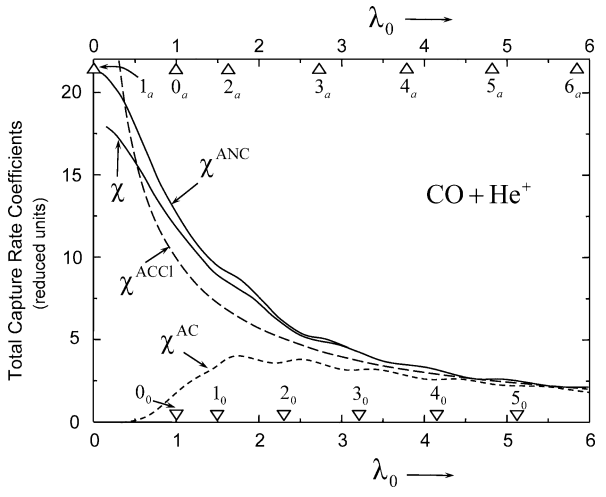

Figure 4. Reduced rate coefficients for $CO + Ar^+$ capture. Shown are accurate ANC, AC, and ACCl rate coefficients, (χ, χ^{ANC}, χ^{AC}, and χ^{ACCl}, respectively) vs λ_0. The symbols J_0, $J = 1, 2, ...$, on the lower λ_0 axis indicate the classical opening of the capture channels for the $v_0^{J,AC,eff}$ potential, while the symbols J_a on the upper λ_0 axis indicate the classical opening of the capture channels for the $v_a^{J,ANC,eff}$ potential.

breaks down completely for $\chi_a^{J,ANC} < 3$ and deviates noticeably from the accurate rate already at $\lambda_0(\kappa) = 4$. For higher values of λ_0, the latter is determined mainly by the isotropic ion-induced dipole interaction (very small value of a) and, therefore, converges to $^1/_3$. We see that the rate coefficients at $\lambda_0 = 6$ are noticeably higher than their asymptotes. The difference between this case and the one presented in Figure 2 is due to a larger quadrupole moment of N_2 compared to that for H_2.

Case 3: $CO + He^+$ *capture, odd case, high anisotropic* $1/R^3$ *interaction, medium anisotropic* $1/R^4$ *interaction, and collision energy below and above the maximum of* v_1^{AC}.

For this system, the AC potentials at large distances resemble those for $N_2 + He^+$ system: attraction in the $\omega = 0$ state and repulsion in the $\omega = 1$ state as a result of the ion−quadrupole interaction. The pattern of curves for the $CO + He^+$ capture is similar to that for the $N_2 + He^+$ capture, except that the rate coefficients are higher in the former case, see Figure 4. This is undoubtedly due to the larger quadrupole moment of CO compared to that of N_2. This difference persists also in the Bethe limit. For large values of b and small enough a, the rate coefficient scales proportional to b (see section 5). Therefore, we have $\chi^B_{CO+He}/\chi^B_{N_2+He} \approx b_{CO+He}/b_{N_2+He} = 1.6$ which agrees with the data from Figure 3 and 4. It is not possible to indicate the high-energy limit of χ^{ACCl}, since it is attained beyond the range of applicability of the perturbed-rotor approximation; even if the latter is adopted, it yields a meaningless result since, at smaller separations (that are important for high energies), the potential v_0 becomes repulsive, and a new capture channel opens for the potential v_1.

Case 4: $HCl + H_3^+$ *capture, even case, high anisotropic* $1/R^3$ *interaction, very high anisotropic* $1/R^4$ *interaction, and collision energy noticeably below the maximum of* v_0^{AC}.

Qualitatively, the pattern of curves, presented in Figure 5, resembles that in Figure 2 for $H_2 + Ar^+$. Quantitatively, the differences are as follows.

(i) The zero-energy rate coefficients for $HCl + H_3^+$ capture are substantially higher than for $H_2 + Ar^+$ capture. We were unable to derive an analytical Bethe limit for the rate coefficient

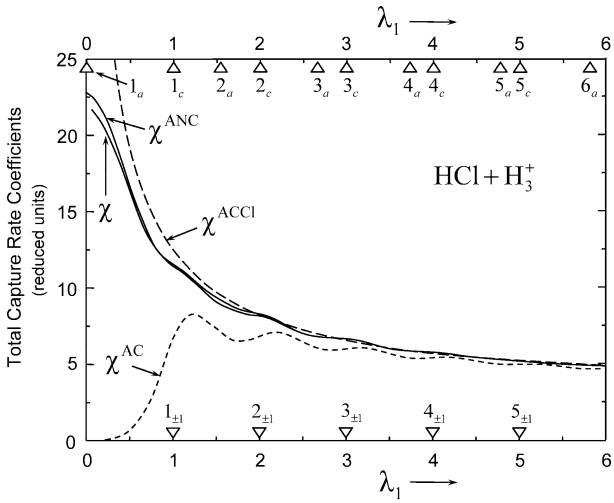

Figure 5. 5. Reduced rate coefficients for the $HCl + H_3^+$ capture. Shown are accurate, ANC, AC, and ACCl rate coefficients, (χ, χ^{ANC}, χ^{AC}, χ^{ACCl}, respectively) vs λ_1. The symbols $J_{\pm1}$, $J = 1, 2, ...$, on the lower λ_1 axis indicate the classical opening of the capture channels for the $v_{\pm1}^{J,AC,eff}$ potentials, while the symbols J_a, J_c on the upper λ_1 axis indicate the classical opening of the capture channels for the $v_a^{J,ANC,eff}$, $v_c^{J,ANC,eff}$ potentials.

using the asymptotic form of the ANC potential, because the latter contains three terms of the form ρ^{-4}, ρ^{-5}, ρ^{-6} with comparable coefficients. However, if in the asymptotic expansion one retains the leading term only (proportional to ρ^{-4}), the rough estimate for the ratio reads $\chi^B_{HCl}/\chi^B_{H_2} \approx b_{HCl}/b_{H_2} \approx 4$. This is consistent with the zero-energy limits of the rate coefficients presented in Figures 2 and 5.

(ii) The capture rate for the $HCl + H_3^+$ encounter is effected by the anisotropic ion-induced dipole-like interaction to a larger degree than the $H_2 + Ar^+$ encounter. The interplay between anisotropic ρ^{-3} and ρ^{-4} interactions can be qualitatively characterized by the ratio $\chi_{\lambda=0}/\chi_{\lambda=6}$ in which the numerator is mainly determined by the ρ^{-3} term while the denominator is determined by the ρ^{-4} term. An increase in the ion-induced dipole-type interaction would decrease this ratio. Indeed, we

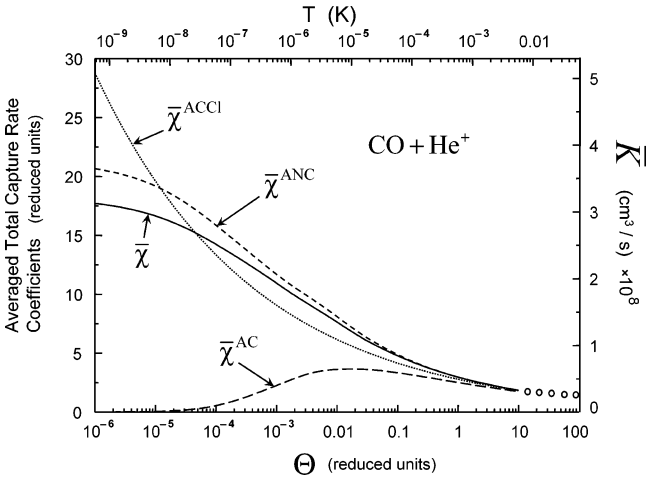

Figure 6. Thermal reduced rate constants for CO + Ar^+ capture vs reduced temperature θ (lower axis) and temperature in kelvin (upper axis). The open circles at the right-hand part of the graphs correspond to the region where the perturbed-rotor approximation may be incorrect. Shown are the accurate, ANC, AC, and ACCl thermal rate constants ($\bar{\chi}$, $\bar{\chi}^{ANC}$, $\bar{\chi}^{AC}$, and $\bar{\chi}^{ACCl}$ respectively).

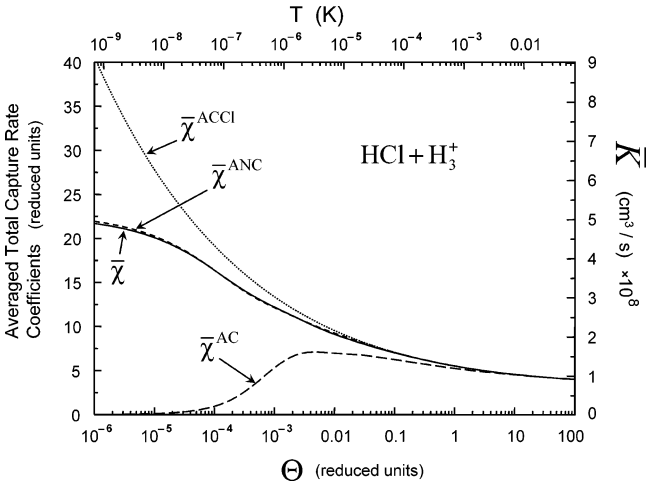

Figure 7. Thermal reduced rate constants for HCl + H_3^+ capture vs reduced temperature θ (lower axis) and temperature in Kelvin (upper axis). Shown are the accurate, ANC, AC, and ACCl thermal rate constants ($\bar{\chi}$, $\bar{\chi}^{ANC}$, $\bar{\chi}^{AC}$, and $\bar{\chi}^{ACCl}$ respectively).

see that this ratio for $H_2 + Ar^+$ is about 6, while for HCl + H_3^+ it is about 4.5.

(iii) The ANC approximation for the HCl + H_3^+ event performs better than for the $H_2 + Ar^+$ event. This can be ascribed to lower radial nonadiabatic coupling in the former case because of the larger spacing between ANC potentials compared to those in the latter case (higher values of a and b for HCl + H_3^+ system compared to that for $H_2 + Ar^+$ system).

It is difficult to indicate the high-energy limit of χ^{ACCl}, since it is attained beyond the applicability of the perturbed-rotor approximation; however, if the latter is adopted it yields the meaningful result $\chi^{ACCl} \rightarrow (^2/_3)\sqrt{1+a}$.

We now consider the temperature-dependent capture rate constants $\bar{\chi}$. They are obtained from χ by averaging over a Maxwell−Boltzmann velocity distribution. This distribution function F, written in terms of the variable κ, reads

$$F(\kappa,\theta)\,\mathrm{d}\kappa = \frac{2\theta^{-3/2}}{\sqrt{2\pi}}\kappa^2 \exp\left(-\frac{\kappa^2}{2\theta}\right)\mathrm{d}\kappa \qquad (44)$$

where the reduced temperature θ is given by

$$\theta = k_B T/E_L \qquad (45)$$

The reduced rate constant assumes the form:

$$\bar{\chi}(\theta) = \int_0^\infty \chi(\kappa)F(\kappa,\theta)\,\mathrm{d}\kappa \qquad (46)$$

with similar definitions for $\bar{\chi}^{ANC}(\theta)$, $\bar{\chi}^{AC}(\theta)$, and $\bar{\chi}^{ACCl}(\theta)$. The results of calculations for $H_2 + Ar^+$ and $N_2 + He^+$ were presented in our recent paper[25] while those for CO + He^+ and HCl + H_3^+ are given in Figures 6 and 7. We see that the ACCl approximation performs well down to, e.g., $T \approx 0.01$ K and that the ANC approximation is quite good for HCl + H_3^+ capture down extremely low temperatures, while it does not work that well for CO + He^+ capture.

Summarizing, we can say that the accurate quantum capture rate coefficients, above the first centrifugal threshold, are adequately represented by the quantum ANC approximation; the latter is reasonably well simulated by the classical AC approximation (convergence of ANC J-thresholds to AC J-thresholds).

The reason, why the classical AC approach performs well at energies where the capture rate coefficients are still determined by partial contributions with low angular momenta quantum numbers, is 2-fold. First, the classical approximation well simulates the compensation of two quantum effects, tunneling through and reflection above centrifugal barriers. Second, the classical approximation, which identifies (erroneously) the expectation value of the square of the total angular momentum with the square of the relative angular momentum, suppresses somewhat too high centrifugal barriers within the quantum AC approach. The additional smoothing of undulations, compared to the capture in the field of an isotropic potential as found in ref 8, is due to the contribution of more partial rate coefficients to the total rate coefficient because of angular momentum recoupling.

Conclusion

On the basis of earlier work on the theory of complex formation or capture processes, we now can characterize the following approaches which are expected to perform progressively better with decrease in the collision energy or temperature.

(i) Fully classical calculations. These are based on classical trajectories in the field of anisotropic potentials, selecting those that lead to complex-formation.

(ii) Classical AC calculations. These are based on the calculation of the AC potentials, and the calculation of classical capture cross sections for isotropic long-range AC potentials.

(iii) Quantum AC calculations. These are based on the calculation of the AC potentials, and the calculation of quantum capture cross sections for isotropic long-range AC potentials.

(iv) Quantum ANC calculations. These are based on the calculation of the ANC potentials, and the calculation of quantum capture cross sections for isotropic long-range ANC potentials.

(v) Fully quantum calculations. These are based on the solution of the coupled scattering Schroedinger equations with absorbing boundary conditions at the complex boundary.

Using four representative systems as examples, we have shown that quantum ANC calculations reproduce quite well the results of accurate quantum calculations in the low-energy collision regime where the perturbed rotor approximation is adequate. This is due to a very weak radial nonadiabatic coupling between the ANC states. Besides, both ANC and

accurate quantum results are reasonably well reproduced by the classical AC calculations provided that several (not too many) partial contributions make up the total rate coefficient. This is due to the artificial simulation of the quantum transmission through the centrifugal barriers by the classical smoothing of individual contributions (replacing the summation over angular momenta by an integration), and the classical suppression of barrier heights (replacing the expectation value of the square of the orbital momentum by its unperturbed classical counterpart).

Acknowledgment. Financial support of this work by the Deutsche Forschungsgemeinschaft (SFB 357 "Molekulare Mechanismen unimolekularer Prozesse") and by the KAMEO program, Israel, is gratefully acknowledged.

References and Notes

(1) Quack, M.; Troe, J. In *Encyclopedia of Computational Chemistry*; Schleyer, P. V., Allinger, N. L., Clark, T., Gasteiger, J., Kollmann, P. A., Eds.; Wiley: Chichester, U.K., 1998; Vol. 4, pp 2708−2726.

(2) Nikitin, E. E.; Troe, J. *Ber. Bunsen-Ges. Phys. Chem.* **1997**, *101*, 445−458.

(3) Maergoiz, A. I.; Nikitin, E. E.; Troe, J.; Ushakov, V. G. *J. Chem. Phys.* **1996**, *105*, 6263−6269. Maergoiz, A. I.; Nikitin, E. E.; Troe, J.; Ushakov, V. G. *J. Chem. Phys.* **1996**, *105*, 6270−6276. Maergoiz, A. I.; Nikitin, E. E.; Troe, J.; Ushakov, V. G. *J. Chem. Phys.* **1996**, *105*, 6277−6284. Maergoiz, A. I.; Nikitin, E. E.; Troe, J.; Ushakov, V. G. *J. Chem. Phys.* **1998**, *108*, 5265−5280; **1998**, *108*, 9987−9998.

(4) Dashevskaya, E. I.; Nikitin, E. E.; Troe, J. *J. Chem. Phys.* **1990**, *93*, 7803−7807.

(5) Nikitin, E. E.; Troe, J.; Ushakov, V. G. *J. Chem. Phys.* **1995**, *102*, 4101−4111.

(6) Berengolts, A.; Dashevskaya, E. I.; Nikitin, E. E.; Troe, J. *Chem. Phys.* **1995**, *195*, 271−281; **1995**, *195*, 283−289.

(7) Maergoiz, A. I.; Nikitin, E. E.; Troe, J.; Ushakov, V. G. *J. Chem. Phys.* **2002**, *117*, 4201−4213.

(8) Dashevskaya, E. I.; Litvin, I.; Maergoiz, A. I.; Nikitin, E. E.; Troe, J. *J. Chem. Phys.* **2003**, *118*, 7313−7320.

(9) Landau, L. D.; Lifshitz, E. M. *Quantum Mechanics*; Pergamon Press: Oxford, U.K., 1977.

(10) Troe, J. *J. Chem. Phys.* **1987**, *87*, 2773−2780.

(11) Takayanagi, K. *J. Phys. Soc. Jpn.* **1978**, *45*, 976−985.

(12) Sakimoto, K. *Chem. Phys.* **1981**, *63*, 419−436; **1984**, *85*, 273−278.

(13) Turulski, J.; Niedzielski, J.; Sakimoto, K. *Chem. Phys.* **1993**, *174*, 387−395.

(14) Bates, D. R. *Proc. R. Soc. London A* **1982**, *384*, 289−300.

(15) Clary, D. C. *Mol. Phys.* **1985**, *54*, 605−618.

(16) Dateo, C. E.; Clary, D. C. *J. Chem. Phys.* **1989**, *90*, 7216−7228.

(17) Dubernet, M. L.; McCarroll, R. *Z. Phys. D* **1989**, *13*, 255−258.

(18) Nikitin, E. E.; Umanskii, S. Ya. *Theory of Slow Atomic Collisions*; Springer: Berlin, 1984.

(19) Smith, S. C.; Troe, J. *J. Chem. Phys.* **1992**, *97*, 5451−5464.

(20) Troe, J. *J. Chem. Phys.* **1996**, *105*, 6249−6262.

(21) Nikitin, E. E.; Troe, J. *J. Chem. Phys.* **1990**, *92*, 6594−6598.

(22) Wigner, E. P. *Phys. Rev.* **1948**, *73*, 1002−1009.

(23) Côté, R.; Friedrich, H.; Trost, J. *Phys. Rev. A* **1997**, *56*, 1781−1787.

(24) Eltschka, C.; Moritz, M. J.; Friedrich, H. *J. Phys. B* **2000**, *33*, 4033−4051.

(25) Dashevskaya, E. I.; Litvin, I.; Nikitin, E. E.; Troe, J. *J. Chem. Phys.*, in press.